A THz imaging system for biomedical applications

A THz Imaging System for Biomedical Applications

T. Rubæk*, R. N. Dahlbäck †, A. Fhager*, J. Stake†, M. Persson*
*Division of Signal Processing and Biomedical Engineering
Department of Signals and Systems
Chalmers University of Technology
SE-412 96 Gothenburg, Sweden
†Terahertz and Millimetre Wave Laboratory
Department of Microtechnology and Nanoscience – MC2
Chalmers University of Technology
SE-412 96 Gothenburg, Sweden

***Abstract*—Imaging using the THz-range of the electromagnetic spectrum is currently emerging as an interesting tool for security, safety, and biomedical applications. In this paper, a THz imaging system designed for biomedical analysis is described. The system consists of a pair of antennas operating in transmission mode at 335 GHz. During measurements the antennas are moved parallel to the sample under investigation while data is collected.**

I. Introduction

In recent years, advances in the development of hardware in the THz region of the electromagnetic spectrum (ranging from 300 GHz to 3 THz) has made imaging and spectroscopy with THz waves a feasible tool for medical applications [1]–[4]. Suggested applications include cancer diagnostics, dental imaging, and wound monitoring [5]–[8].

In the THz region, the interactions between the electromagnetic fields and biological tissue is to a large extent governed by the high absorbance of water. This allows for easily identifying tissues with different water content, e.g., healthy and cancerous tissue [9]–[11]. It does, however, also severely limits the penetration of the electromagnetic field through the tissue, implying that only the outermost few mm of the tissue can be examined [6]. For tissues with low a content of free water, such as teeth and bone, the penetration depth is much greater [4], [12].

In addition to imaging, spectroscopy in the THz region has also found use in biomedical applications since a number of proteins and other interesting molecules have resonances in the this part of the frequency spectrum [13], [14].

The most widespread form of THz imaging today is pulsed THz imaging in which a short pulse (having a wide bandwidth) is used to image the sample. The imaging system can be configured either for transmission measurements with the sample under investigation positioned between the transmitting and receiving antennas [15], or in reflection mode with the transmitter and receiver positioned on the same side of the system [16], [17].

The cross-range resolution in such systems is most commonly determined by the beam width of the antenna while the depth-resolution is determined by the pulse width.

Instead of using a wideband pulse, it is also possible to do imaging by using a single frequency – a technique which is also known as continuous wave (CW) imaging. In such systems, the information which is contained in the multiple frequencies of the broadband imaging system must be retrieved by combining different transmitter and receiver combinations.

At Chalmers University of Technology, a CW imaging system is currently being developed. The intended use of the system is biomedical imaging and diagnostics and the system is operating in transmission mode. In this paper, the individual parts of the system are described. This includes the overall system design, the THz hardware, the antennas, and the imaging algorithm.

II. System Design

A photo of the system is shown in Fig. 1. The system consists of three parts: A high-frequency circuit capable of transmitting a CW signal on the transmitting channel while measuring the resulting amplitude and phase on the receiving channel; a mechanical setup capable of scanning the transmit and receive antennas independent of each other at opposite sides of the sample to be investigated; and finally a computer which controls the data acquisition process.

The mechanical axes are controlled by stepper motors and are capable of moving the antennas in two parallel planes. The area in which the antennas can be moved covers an area of approximately 150 mm by 150 mm in steps of 2.5 μm and the repeatability has been measured to be in the same order (2.5 μm).

III. THz Hardware

A block diagram of the THz hardware of the imaging system is shown in Fig. 2. The hardware consists of two high-frequency chains, one for the transmitting and one for the receiving antenna, and an IF circuit.

In the transmit chain, the high-frequency signal is achieved by multiplication through a $\times 5$ HBV multiplier and a $\times 2$ Schottky multiplier, yielding a total multiplication factor of 10. In the receiver chain, the

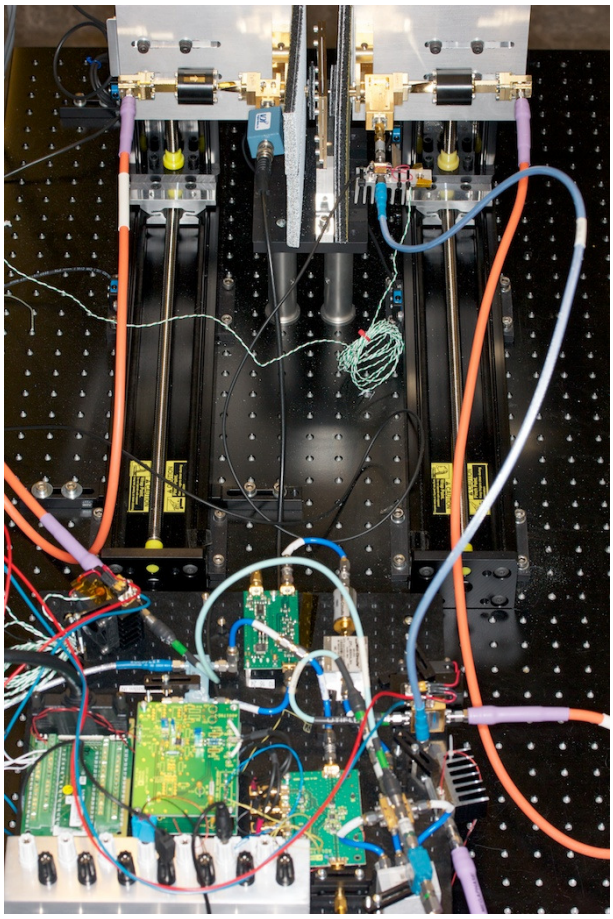

Fig. 1: Photo of the imaging system. The IF hardware can be seen in the bottom of the photo while the frequency doublers and antennas are mounted on the movable axes in the top of the photo.

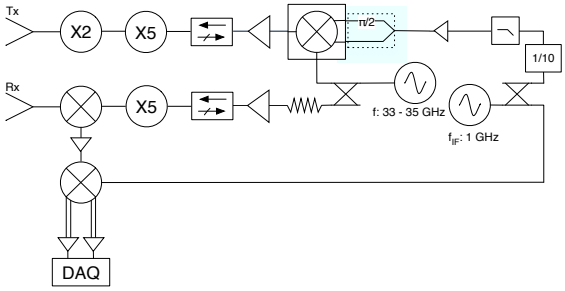

Fig. 2: Block diagram of the THz imaging system. The signal to the transmitter antenna is send through a $\times 5$ HBV multiplier and a $\times 2$ Schottky-based multiplier for a total multiplication factor of 10. The multiplication in the receiver chain is achieved with a $\times 5$ HBV multiplier and a second-harmonic mixer.

Fig. 3: Photo of the antennas used in the system. The antennas are open-ended waveguides and the walls of the waveguides have been cut in a 45° to minimize the effects of standing waves between the fronts of the antennas. For the same reason, absorbers (seen as gray and black material on the photo) are mounted around and behind the antennas.

multiplication is achieved by a $\times 5$ HBV multiplier and a second-harmonic Schottky-based mixer.

The high-frequency chains are designed for an input signal with a frequency between 33 and 35 GHz which, after the multiplication, yields a frequency between 330 and 350 GHz to be used for the imaging. As the change in wavelength and penetration depth in this frequency interval is minuscule, the actual operating frequency is chosen to be 335 GHz since the system has its optimum performance at this frequency.

The IF signal has a frequency of 1 GHz and is send through a frequency divider with a division ratio of 10 before it is mixed into the input signal to the transmit chain. Since the signal is multiplied by a factor of 10 in the transmit chain, the output signal of the second-harmonic Schottky mixer in the receive chain will have the same frequency as the IF input.

The total available output power at the terminal of the transmitting antenna is approximately 0.5 mW and the noise floor has been estimated to be more than 60 dB below this level.

IV. Antennas

The antennas used in the system are simple open-ended waveguides based on standard rectangular WR-2.8 waveguides. A photo of the antennas is shown in Fig. 3. The dimensions of the waveguides are 0.710 mm by 0.355 mm and to achieve the necessary mechanical stability in the system, the walls of the waveguides are 0.5 mm thick. The relatively thick walls implies that it has been necessary to cut the front of the waveguides in a 45° angle to eliminate the standing waves that would otherwise arise when two such relative large metallic surfaces are placed opposite of each other.

To further minimize the effects of the standing waves, absorbers have been placed behind and around the antennas. These can be seen as the gray and black

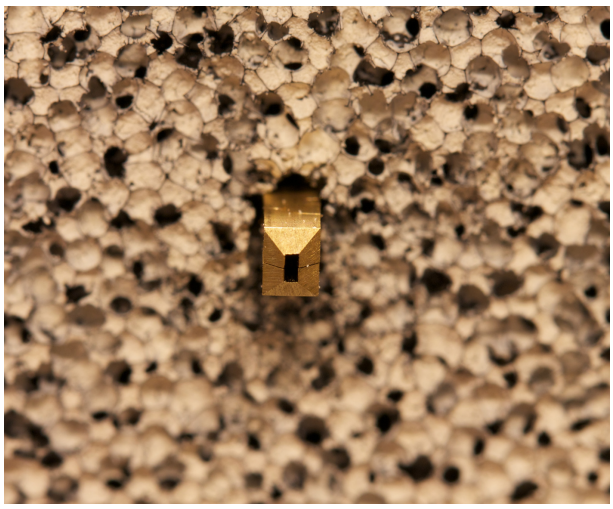

Fig. 4: Close-up of one of the antennas in the system. The opening of the waveguide measures 0.355 mm by 0.710 mm and the walls of the waveguide has a thickness of 0.500 mm.

slabs in Fig. 3 and as the gray background in Fig. 4, wherein a front view of a single antenna is shown. By surrounding the antennas with absorbers in this manner, the influence of the surroundings is effectively eliminated and the antennas behaves as if they are positioned in free space.

The antennas are characterized by a rather broad radiation pattern. The 3 dB beam width in the farfield is approximately 110° by 70° and although the antennas are not used in the farfield, this gives a good indication of the width of the beam of the antennas.

Although such a broad beam is usually avoided in wideband imaging systems, the broad beam is advantageous when doing CW imaging since it allows for the transmitter and receiver to see the same region of the sample under test from multiple angles. Something which is not easily achieved with antennas with a narrow beam.

V. Imaging Algorithm

The imaging algorithm used in the system is based on a reconstruction of the electromagnetic parameters, i.e., permittivity and conductivity, of the sample under investigation.

The measured complex signal $S_{r,t}$ for a given position of the transmit and receive antennas (indicated by the subscript r, t) can be divided into two components: One originating from the incident field and one from the scattered field. The incident field is the field which is present in the system when there is no sample in the system, and the scattered field is the field which arises when a sample is positioned in the system. The signal can thus be expressed as:

$$S_{r,t}^{\text{tot}} = S_{r,t}^{\text{inc}} + S_{r,t}^{\text{sct}} \tag{1}$$

wherein $S_{r,t}^{\text{tot}}$ is the total measured signal, $S_{r,t}^{\text{inc}}$ is the part of the signal originating from the incident field, and $S_{r,t}^{\text{sct}}$ is the part of the signal originating from the scattered field.

By introducing the object function

$$O(\boldsymbol{r}) = \Delta\sigma(\boldsymbol{r}) - i\omega\Delta\epsilon(\boldsymbol{r}) \tag{2a}$$

the scattered field from a given object can be expressed as

$$\boldsymbol{E}^{\text{sct}} = i\omega\mu_0 \int_V \bar{\bar{\boldsymbol{G}}}(\boldsymbol{r}, \boldsymbol{r'}) \cdot \boldsymbol{E}^{\text{tot}}(\boldsymbol{r'}) O(\boldsymbol{r'}) \, \mathrm{d}\boldsymbol{r'}. \tag{2b}$$

In these expressions $\boldsymbol{r}$ and $\boldsymbol{r'}$ are position vectors, $\bar{\bar{\boldsymbol{G}}}$ is the dyadic Green's function, and $\boldsymbol{E}^{\text{sct}}$ and $\boldsymbol{E}^{\text{tot}}$ are the scattered and total electric field, respectively. The object function O is given by the contrast in conductivity σ and permittivity ϵ between the object and the background, i.e.,

$$\Delta\sigma(\boldsymbol{r}) = \sigma(\boldsymbol{r}) - \sigma_{\text{bg}} \tag{3a}$$

and

$$\Delta\epsilon(\boldsymbol{r}) = \epsilon(\boldsymbol{r}) - \epsilon_{\text{bg}}. \tag{3b}$$

By application of the reciprocity theorem (see e.g. [18]) it can be shown that the change in the measured signal caused by the presence of a scatterer can be expressed as

$$S_{r,t}^{\text{sct}} = \alpha \int_V \boldsymbol{E}^{\text{trans}}(\boldsymbol{r'}) \cdot \boldsymbol{E}^{\text{rec}}(\boldsymbol{r'}) O(\boldsymbol{r'}) \, \mathrm{d}\boldsymbol{r'} \tag{4}$$

wherein α is a constant which is dependent on various parameters of the system setup, such as how the antennas are fed. This constant can be determined either through analysis of the system or by a simple calibration measurement of a known target.

The two fields $\boldsymbol{E}^{\text{trans}}(\boldsymbol{r'})$ and $\boldsymbol{E}^{\text{rec}}(\boldsymbol{r'})$ are the fields at the point $\boldsymbol{r'}$ when the transmitting or the receiving antenna, respectively, are transmitting.

Thus, the expression in (4) allows for setting up an equation system which can be solved for the unknown distribution of the object function. For small targets or targets with low contrast, the expression in (4) can be solved as a set of linear equations wherein the fields $\boldsymbol{E}^{\text{trans}}(\boldsymbol{r'})$ and $\boldsymbol{E}^{\text{rec}}(\boldsymbol{r'})$ are assumed to be equal to those of the empty system. By discretizing the volume in which the sample under investigation is positioned and scanning the transmitting and receiving antennas to several different locations, the matrix equation

$$\underline{\underline{E}}\,\underline{O} = \underline{S} \tag{5}$$

can be constructed. Herein $\underline{\underline{E}}$ is a matrix consisting of the products of the fields for each of the cells of the discretized volume, $\underline{O}$ is a column vector holding the unknown values of the object function, and $\underline{S}$ is a column vector holding the measured signals.

For larger samples or for samples with high contrast, the assumption that the fields are not significantly influenced by the presence of the sample does not hold and the inversion problem must be solved iteratively using a procedure similar to that outlined in [18].

REFERENCES

[1] B. B. Hu and M. C. Nuss, "Imaging with terahertz waves," *Optics Letters*, vol. 20, no. 16, p. 1716, 1995.

[2] P. Siegel, "Terahertz technology in biology and medicine," *Microwave Theory and Techniques, IEEE Transactions on*, vol. 52, no. 10, pp. 2438–2447, 2004. [Online]. Available: 10.1109/TMTT.2004.835916

[3] D. Woolard, R. Brown, M. Pepper, and M. Kemp, "Terahertz frequency sensing and imaging: A time of reckoning future applications?" *Proceedings of the IEEE*, vol. 93, no. 10, pp. 1722–1743, 2005. [Online]. Available: 10.1109/JPROC.2005.853539

[4] E. Pickwell and V. P. Wallace, "Biomedical applications of terahertz technology," *Journal of Physics D: Applied Physics*, vol. 39, no. 17, pp. R301–R310, 2006.

[5] T. Lffler, K. Siebert, S. Czasch, T. Bauer, and H. G. Roskos, "Visualization and classification in biomedical terahertz pulsed imaging," *Physics in Medicine and Biology*, vol. 47, pp. 3847–3852, 2002.

[6] R. M. Woodward, V. P. Wallace, D. D. Arnone, E. H. Linfield, and M. Pepper, "Terahertz pulsed imaging of skin cancer in the time and frequency domain," *Journal of Biological Physics*, vol. 29, no. 2, p. 257259, 2003.

[7] Z. D. Taylor, R. S. Singh, M. O. Culjat, J. Y. Suen, W. S. Grundfest, H. Lee, and E. R. Brown, "Reflective terahertz imaging of porcine skin burns," *Optics Letters*, vol. 33, no. 11, pp. 1258–1260, Jun. 2008.

[8] J. Son, "Terahertz electromagnetic interactions with biological matter and their applications," *Journal of Applied Physics*, vol. 105, no. 10, p. 102033, 2009. [Online]. Available: http://link.aip.org/link/JAPIAU/v105/i10/p102033/s1&Agg=doi

[9] A. J. Fitzgerald, E. Berry, N. N. Zinov'ev, S. Homer-Vanniasinkam, R. E. Miles, J. M. Chamberlain, and M. A. Smith, "Catalogue of human tissue optical properties at terahertz frequencies," *Journal of Biological Physics*, vol. 29, no. 2, p. 123128, 2003.

[10] A. J. Fitzgerald, V. P. Wallace, M. Jimenez-Linan, L. Bobrow, R. J. Pye, A. D. Purushotham, and D. D. Arnone, "Terahertz pulsed imaging of human breast tumors," *Radiology*, vol. 239, no. 2, p. 533, 2006.

[11] H. Hoshina, A. Hayashi, N. Miyoshi, F. Miyamaru, and C. Otani, "Terahertz pulsed imaging of frozen biological tissues," *Applied Physics Letters*, vol. 94, no. 12, p. 123901, 2009. [Online]. Available: http://link.aip.org/link/APPLAB/v94/i12/p123901/s1&Agg=doi

[12] D. Arnone, C. Ciesla, M. Pepper *et al.*, "Terahertz imaging comes into view," *Physics World*, vol. 4, p. 3540, 2001.

[13] H. H. Mantsch and D. Naumann, "Terahertz spectroscopy: The renaissance of far infrared spectroscopy," *Journal of Molecular Structure*, vol. 964, no. 1-3, pp. 1–4, Feb. 2010.

[14] T. Globus, "Optical characteristics of biological molecules in the terahertz gap," in *Proceedings of SPIE*, Philadelphia, PA, USA, 2004, pp. 1–10. [Online]. Available: http://link.aip.org/link/?PSI/5584/1/1&Agg=doi

[15] C. Chiu, H. Chen, Y. Huang, W. Lee, Y. Hwang, H. Huang, and C. Sun, "All-terahertz fiber-scanning near-field microscopy," *Optics Letters*, vol. 34, no. 7, pp. 1084–1086, 2009.

[16] R. M. Woodward, B. E. Cole, V. P. Wallace, R. J. Pye, D. D. Arnone, E. H. Linfield, and M. Pepper, "Terahertz pulse imaging in reflection geometry of human skin cancer and skin tissue," *Physics in Medicine and Biology*, vol. 47, p. 38533863, 2002.

[17] C. B. Reid, E. Pickwell-MacPherson, J. G. Laufer, A. P. Gibson, J. C. Hebden, and V. P. Wallace, "Accuracy and resolution of THz reflection spectroscopy for medical imaging," *Physics in Medicine and Biology*, vol. 55, no. 16, pp. 4825–4838, 2010. [Online]. Available: http://iopscience.iop.org/0031-9155/55/16/013

[18] T. Rubaek, O. S. Kim, and P. Meincke, "Computational validation of a 3-D microwave imaging system for Breast-Cancer screening," *IEEE Transactions on Antennas and Propagation*, vol. 57, no. 7, pp. 2105–2115, 2009.